

Extracting Shape and Reflectance of Glossy Surfaces by Using 3D Photometric Sampling Method

Hideichi Sato Shree K. Nayar Katsushi Ikeuchi

The Robotics Institute
Carnegie Mellon University
Pittsburgh, PA 15213

Abstract

The photometric sampling method [4] extracts shape and reflectance properties of surfaces (Lambertian, specular, and hybrid) by using multiple illumination directions and a single viewing direction. This paper describes a complete implementation and a performance evaluation of a three-dimensional version of the photometric sampler. The experimental conducted on Lambertian surfaces, specular surfaces, and hybrid surfaces show high accuracy in both estimated orientations as well as reflectance parameters.

Introduction

Surface shape and roughness are important inspection criteria in many industrial applications. In particular, surface reflectance properties can be interpreted as measures of surface roughness. We have presented the photometric sampling [4] for determining the shape and reflectance of objects. A sequence of images of the object are generated by actively controlling an array of sources, which are located on a plane passing through the object. Surface reflectance as well as orientation are determined from the image sequence. However, we had only implemented and demonstrated 2D version of the photometric sampling method: all of the light sources were located in the same plane and only objects with translated symmetry could be handled.

This paper describes the extension of our previous work, a 3D version of the photometric sampling which can handle surfaces of arbitrary shape. Surface orientation is extracted without prior knowledge of the relative strengths of the Lambertian and specular reflection components. The method also determines the parameters of the reflectance model at each surface point. The experimental results have shown high accuracy in extracted object shape and surface reflectance properties.

Extended Source

We use extended light sources to illuminate the object surface [2]. Unlike a point source, an extended source emits light

from an area of points rather than a single point. This characteristic of an extended source reduces the number of necessary sources to detect specular components of reflection.

We generate an extended source by illuminating a sphere made of light-diffusing material with a point source of light. The object is placed at the center of the spherical diffuser and is viewed by the camera through a hole in the diffuser. In the following discussion, the origin of the viewer center coordinate system is defined as the sphere center, and the Z axis corresponds to the optical axis of the TV camera. All vectors, such as \vec{S} and \vec{N} , are defined in this viewer centered coordinate system.

By using the radius of the sphere, R , and the distance between a point light source and the sphere, H , we can express the brightness distribution function of an extended light source as

$$L(\vec{P}, \vec{S}; R, H) = \frac{C[(R+H)(\vec{S} \cdot \vec{P}) - R]}{[(R+H - R(\vec{S} \cdot \vec{P}))^2 + (R(1 - (\vec{S} \cdot \vec{P}))^2)]^{\frac{3}{2}}} \quad (1)$$

where \vec{P} denotes a unit vector to a point on the diffuse surface from the sphere center and \vec{S} denotes the point light source direction from the sphere center.

The brightness distribution in the image of an object is closely related to the reflectance properties and shape of the object surface, and the characteristics of the light source used to illuminate the object. The image irradiance equation is defined as one that relates image brightness to the surface reflectance and the imaging geometry: surface orientation, viewer and source direction. The equation for surface illumination by the extended source is:

$$I' = A' \vec{N} \cdot \vec{S} + B' L(\vec{S}_n(\vec{N}), \vec{S}; R, H), \quad (2)$$

where A' and B' are the Lambertian and specular strength of the point, and \vec{N} and \vec{S} are the surface orientation and the source direction. $\vec{S}_n(\vec{N})$ denotes the specular source direction which gives the specular reflection to the viewer at the surface of the orientation, \vec{N} .

The area of the image irradiance equation containing specular brightness is bounded by an α radius circle. This termination angle α is related to the distance H between a point source and the surface of the diffuser:

$$\cos \alpha = \frac{R}{R+H}, \quad (3)$$

where R denotes the radius of the diffuser.

¹This research was conducted in the Task-oriented Vision Laboratory, the Robotics Institute, Carnegie Mellon University. Image Understanding Research in the TVL is supported in part by the Westinghouse Electric Corporation and in part by the Defense Advanced Research Project Agency, DOD, through ARPA order No. 4976, and monitored by the Air Force Avionics Laboratory under contract F33615-87-C-1499. Hideichi Sato was on leave of absence from Komatsu Ltd., Kanagawa, Japan. Takeo Kanade provided many useful comments and encouragements.

Photosampler Apparatus

The process of measuring image brightness for different source directions is equivalent to sampling the image irradiance equation, $I'(\vec{S})$, at various \vec{S}_i . We distribute an array of extended sources around the object such that each source illuminates the object from a different direction. The entire array of extended sources may be scanned by sequentially activating each source one at a time and taking an image. Therefore, the scanning process results in a set of brightness, $I_i : i = 1, \dots, M$, measured at each point on the object surface. M equals the number of extended sources.

Uniform sampling of the image irradiance equation may be obtained by distributing extended sources in a tessellation that results from projecting onto the unit sphere a regular polyhedron whose center coincides with that of the sphere[1]. A higher frequency polyhedron which consists of triangular faces can be used [6] for a smaller meshed tessellation.

We will use a polyhedron whose edge length projects to an arc length equivalent to α . This spacing allows the image irradiance equation to be uniformly sampled at an interval equal to α . Under this sampling interval, one and only one spherical triangle gives three non-zero specular brightness. We will use this constraint for designing a recovery algorithm. We will refer to this triangle and the constrain as the *specular triangle* and the *sampling constraint*, respectively.

Figure 1 shows a photograph of the experimental device. A 355.6mm (14-inch) diameter lamp shade is used as the spherical diffuser. Extended light sources are generated on the diffuser's surface by illuminating it with 36 60W frosted incandescent light bulbs. The bulbs are located at 36 of the 42 vertices of one-frequency icosahedron². The object is placed at the center of the diffuser and is viewed by a camera through a 25.4mm (1-inch) diameter hole in the surface of the diffuser. The complete imaging system, comprise of lenses and camera, has a physical resolution of 0.5mm (0.002 inches) per pixel width.

System Parameters

The system parameters needed to describe the apparatus in details include: light source directions, brightness distribution parameters, and device characteristic parameters. These parameters will be used for determining shape and reflectance properties of unknown objects.

- The *light source directions* represent directions of the center of the light sources denoted by $\vec{S}_i : i = 1, \dots, 36$.
- The *brightness distribution parameters*, C, H , characterize the shape of the brightness distribution of a light source on the diffuser.
- Device characteristic parameters
 - The *base value for specular surfaces* (E_{spec}) represents the increase in brightness due to interreflections inside the diffuser. We assume that this increment is independent on surface orientations.

²A small section of the bottom hemisphere of the diffuser is not illuminated as light sources. This area is not observable from the TV camera.

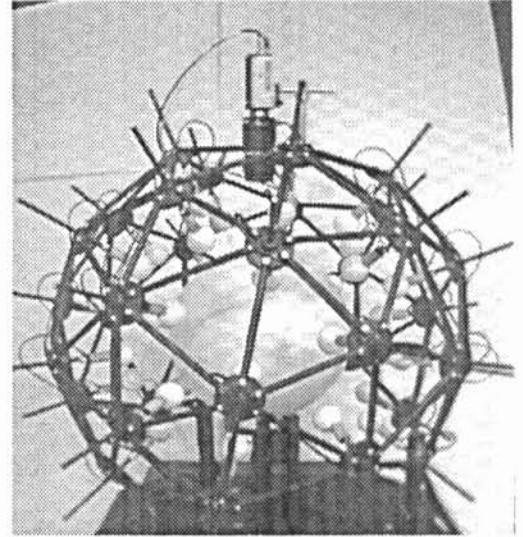


Figure 1: Photograph of the experimental apparatus.

- The *base value for Lambertian surfaces* (E_{lamb}) represents the increase in brightness on Lambertian surface due to interreflections inside of the diffuser. We assume that this increment is also independent on surface orientations. This factor corresponds to the integration of the previous factor over the hemispherical directions.
- The *light source brightness for the pure Lambertian surface* (A'_{max}) represents the brightness that an effective point source would have, in order to produce the same brightness as an extended source.
- The *base value due to defocus effect* (E_{def}) represents the increase in brightness over the entire image because the camera observes a part of the diffuser and blurs that part over the image.

We determine the system parameters and lookup tables for specular component, used in step 3 of extraction procedure mentioned below, by a calibration method. The system parameters, except for E_{def} , are determined for each extended light source. The lookup tables are determined for each triangle on the one-frequency icosahedron. See [5] for more details.

Extraction Procedure

Image brightness at each pixel under the extended light source i can be represented using the system parameters as:

$$I_i(\vec{N}, A', B') = A'(\vec{N} \cdot \vec{S}_i + E_{lamb}) + B'(L'(\vec{S}_i, \vec{N}), \vec{S}_i; R, H) + E_{spec} + E_{def} \quad (4)$$

Step 1: Cosine curve fitting A measured brightness value, I_i includes the three kinds of base values: Lambertian (E_{lamb}), specular (E_{spec}), and defocus (E_{def}). We subtract these base values from the brightness.

$$I'_i = I_i - E_{lamb}A' - E_{spec}B' - E_{def}$$

In the initial iteration, A' and B' are unknown. Therefore, we set $A' = 0$ and $B' = 0$. After second iteration, we will substitute the values obtained at the previous iteration.

Then, the brightness is normalized by the the light source brightness for the pure Lambertian surface, $A'_{max,i}$, of source i to compensate for the difference between the light sources. This step gives the Lambertian strength, A' and surface orientation given by the Lambertian component, \vec{N}_{lamb} .

Step 2: Specular triangle determination We subtract the base value and the Lambertian brightness values, extracted in the former step, from the measured brightness. We obtain the specular brightness as follows:

$$I''_i = I_i - A' \vec{S}_i \cdot \vec{N}_{lamb} - A' E_{lamb} - E_{def}.$$

Three source directions, giving three largest specular brightness values, form the specular triangle.

Step 3: Table lookup The previous procedure gives the specular triangle, i.e. three specular brightness values, I''_1, I''_2, I''_3 . These three values and their corresponding source directions, $\vec{S}_1, \vec{S}_2, \vec{S}_3$ must satisfy the following four equations:

$$\begin{aligned} I''_1 &= B' L(\vec{S}_1(\vec{N}), \vec{S}_1) \\ I''_2 &= B' L(\vec{S}_2(\vec{N}), \vec{S}_2) \\ I''_3 &= B' L(\vec{S}_3(\vec{N}), \vec{S}_3) \\ |\vec{N}| &= 1 \end{aligned} \quad (5)$$

By solving these four equations, we can determine the surface orientation, \vec{N} , and specular strength, B' at each point. In the actual implementation, we use a lookup table to convert a triple of brightness values into a unique surface orientation [5]. This step gives the specular strength, B' and the surface orientation given by the specular component, \vec{N}_{spec} .

Step 4: Orientation We iterate step 1 through step 3 several times to obtain the converged results. We have two surface orientations given by two different methods (Lambertian and specular). We compute a weighted average of both surface orientations into a single value based on the ratio of Lambertian and specular strength:

$$\vec{N} = \frac{A' \vec{N}_{lamb} + B' \vec{N}_{spec}}{A' + B'}.$$

Experimental Results

This section describes experiments conducted to evaluate the performance of the photosampling method. In order to evaluate the accuracy of the method, first, we measure the surfaces of known shape (sphere) and known reflectance (specular). Then, we applied the method to other interesting surfaces to demonstrate the feasibility of the method in practical applications as well as to investigate its limitations. See [5] for more detailed results.

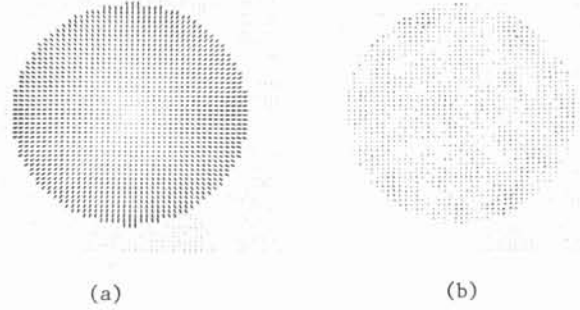


Figure 2: Needle map for the specular ball; (a) Needle map; (b) Needle map for the orientation error of the specular ball: the needle size is enhanced in 15 times;

Specular spherical surface

The 36 images of a 0.5 inch diameter specular ball are obtained using the photo-sampling device. By applying the extraction procedure to these images, we obtain the Lambertian strength and the specular strength. The surface orientation distribution is obtained as shown in Figure 2(a), where a small needle depicts the orientation at that pixel. We find that the errors are less than 1 degree in the central region of the ball.

Figure 2(b) shows the distribution of the errors in computed surface orientations. The figure indicates that the peripheral area has larger error than the central area. This tendency can be explained by the discrepancy of the actual brightness distribution of a light source from the theoretical one.

We can also observe the systematic error distribution over the ball corresponding to the tessellations. The accuracy of an obtained surface orientation is related to the gradient of a brightness distribution function of an extended light source. A steeper portion of the function gives a more accurate orientation. The gradient of the source distribution function is not constant over a triangle. It becomes relatively flat around the peripheral area of a triangle. Consequently, errors increase in that region. Therefore, it is desirable for the function to have a steep gradient at the peripheral area of a triangle. In order to achieve this condition, we should have a larger α than the width of a triangle.

Dip switch

A dip switch, shown in Figure 3(a), is an example of the plastic object with a complicated shape. Figure 3(b) shows the Lambertian strength, Figure 3(c) shows the specular strength. As we expected, the system successfully obtained constant Lambertian strength distribution over the complicated shape. Although the switch has two different albedo areas, the distribution of the surface normals, depicted as the needle map in Figure 3(d), is

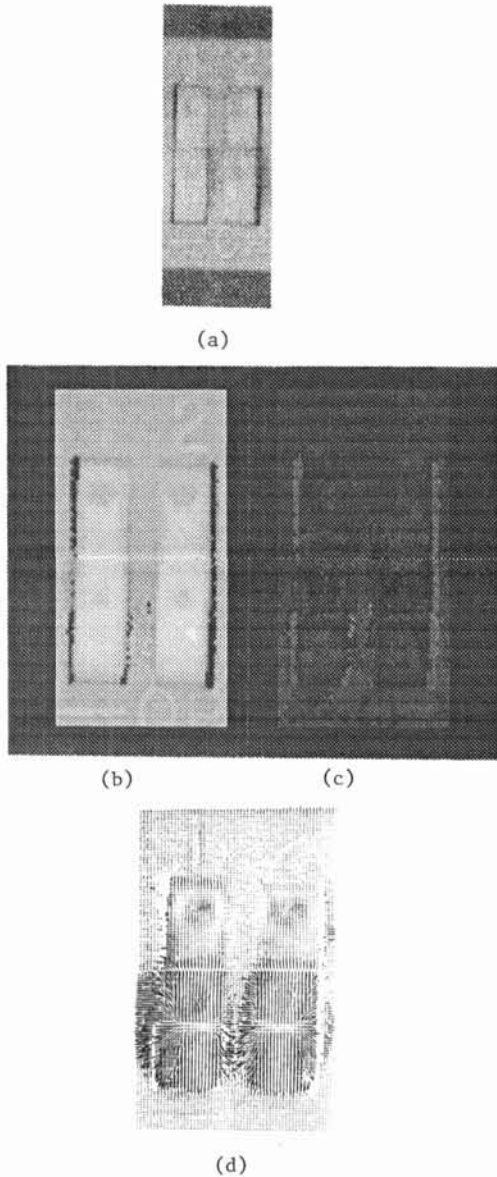


Figure 3: Dip switch: (a) Picture of a dip switch; (b) Lambertian strength image; (c) Specular strength image; (d) Needle map of the dip switch.

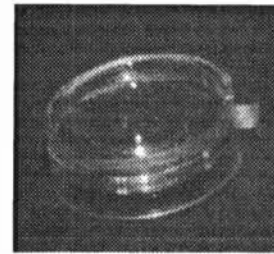
seen not to be influenced by this albedo variation. However, concave and side areas are not detected correctly due to the occlusion. For example, the small circular concave on the switch is extracted with smaller albedo than actual, while the adjacent part to the switch is detected with inaccurate surface normal.

Transparent surface

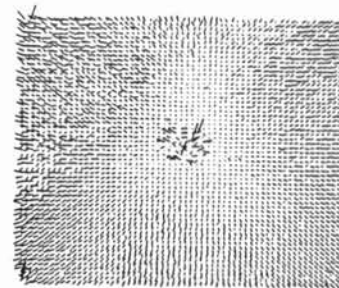
Transparent objects do not have a Lambertian component, but do have a specular component. As an example of a transparent surface, we have used the surface of a plastic lens as shown in Figure 4(a)

The plastic lens causes double reflections; a light ray hits the surface from the air to the plastic lens and a penetrated light ray hits the back surface from the plastic to the air.

In order to measure the only front reflection, we paint the lower surface with dull black spray. Figure 4(b) shows the result. Here, the length of each needle is multiplied by 5 times. The



(a)



(b)

Figure 4: Plastic lens: (a) Picture of a plastic lens; (b) Needle map of the plastic lens.

errors at the center is due to the hole of TV camera.

Conclusions

This paper describes a three-dimensional photometric sampling method to determine shape and reflectance of glossy surfaces by measuring image brightness under various light source directions and viewing from a single direction. The experimental results for Lambertian surfaces, specular surfaces, and hybrid surfaces show high accuracy in both orientations and reflectance parameters.

References

- [1] C. Brown. Fast display of well-tessellated surfaces. *Computer and Graphics*, 4(4):77–85, April 1979.
- [2] K. Ikeuchi. Determining surface orientation of specular surfaces by using the photometric stereo method. *IEEE Trans. Pattern Analysis and Machine Intelligence*, PAMI-3(6):661–669, November 1981.
- [3] K. Ikeuchi and K. Sato. Determining reflectance parameters using range and brightness images. In *Proc. of Intern. Conf. on Computer Vision*, Osaka, JAPAN, December 1990. a longer version is available as CMU-CS-90-106.
- [4] S.K. Nayar, K. Ikeuchi, and T. Kanade. Extracting shape and reflectance of lambertian, specular, and hybrid surfaces. Technical Report CMU-RI-TR-88-14, Carnegie Mellon University, Robotics Institute, August 1988.
- [5] H. Sato, K. Nayar, and K. Ikeuchi. Implementation and evaluation of a three-dimensional photometric sampler. Technical report, The Robotics Institute, 1990. in preparation.
- [6] M.J. Weninger. *Spherical Models*. Cambridge Univ. Press, Cambridge, UK, 1979.